3D light-sheet fluorescence microscopy in preclinical and clinical drug discovery

Urmas Roostalu *, **Henrik H. Hansen**, **Jacob Hecksher-Sørensen**

Gubra, Hørsholm, Denmark

Light-sheet fluorescence microscopy (LSFM) combinedwith tissue clearing has emerged as a powerful technology in drug discovery. LSFM is applicable to a variety of samples, from rodent organs to clinical tissue biopsies, and has been used for characterizing drug targets in tissues, demonstrating the biodistribution of pharmaceuticals and determining their efficacy and mode of action. LSFM is scalable to high-throughput analysis and provides resolution down to the single cell level. In this review, we describe the advantages of implementing LSFM into the drug discovery pipeline and highlight recent advances in this field.

Keywords: light sheet fluorescence microscopy; preclinical imaging; biodistribution imaging; neuronal activation; neurodegenerative diseases; vasculature imaging; preclinical tumor imaging

Introduction

Diverse imaging methods have had a pivotal role in drug discovery, offering valuable insight into the complex mechanisms underlying diseases and the efficacy of potential therapeutics. In preclinical settings, *in vivo* imaging has been extensively used to evaluate pharmacokinetic (PK) drug properties and therapeutic efficacy across a variety of disease models. *In vivo* imaging modalities have often been combined with histological analyses to characterize drug target localization and drug efficacy at a higher resolution. Depending on the study aim, magnetic reso-

Urmas Roostalu is the 3D imaging department manager at Gubra. Research in his team is focused on developing and implementing light sheet microscopy methods for early-stage drug discovery, with emphasis on brain, metabolic, and cardiovascular diseases. He is interested in the development of automated high-throughput imaging platforms for rapid screening of drug candidates. He holds a PhD from the University of Heidelberg on imaging in the context of muscle disorders and has worked at King's College London, University College London, and at the University of Manchester on immunology, translational stem cell research, and vascular biology.

Henrik H. Hansen is scientific director at Gubra, heading medical writing. He holds a PhD in neuroscience from the University of Copenhagen. Given his additional scientific advisory role in the company, he is involved in crossdisciplinary research projects focusing on metabolic, fibrotic, and central nervous system diseases. The overarching aim of his research is to qualify preclinical target and drug discovery by establishing and validating translational disease models.

Jacob Hecksher-Sørensen is a director at Gubra, heading an imaging facility that enables 3D imaging of whole-mouse organs at the single cell level. He holds a PhD in developmental biology from the University of Edinburgh and his current research focuses on understanding how metabolism is regulated by the brain. This includes quantification of drug responses in the brain and detection of fluorescently labeled peptides and antibodies. His aim is to use this knowledge to better understand how metabolism is regulated and to translate these findings into new therapies.

* *Corresponding author. Roostalu, U. (uro@gubra.dk)*

https://doi.org/10.1016/j.drudis.2024.104196

nance imaging (MRI), positron emission tomography (PET), and histology analysis of tissue sections are commonly used in combination with different laboratory assays for characterizing clinical-stage drugs. In recent years, tissue clearing techniques coupled with 3D LSFM have emerged as novel tools in both preclinical and clinical drug development. These methodologies enable imaging of intact tissues and whole organs at cellular resolution, thereby bridging the gap between traditional *in vivo* imaging modalities and *ex vivo* microscopy. Recent advances in 3D LSFM have increased imaging resolution and speed and significantly expanded the variety of targets and endpoints that are possible to image. With the incorporation of state-of-the-art, high-resolution 3D imaging methods in preclinical research workflows, it is now possible to address research questions that had remained difficult, if not impossible, to answer using traditional imaging modalities. As a result, LSFM is now applied across the different stages of drug development, from mapping the expression of drug targets and assessing the mode of action of drug candidates to evaluating therapeutic and adverse effects in patient samples (Figure 1).

LSFM compared with other imaging modalities

A variety of imaging methods have been developed to support the drug discovery process, with the choice depending on the scope of the study (Figure 2). *In vivo* imaging modalities, including PET, MRI, computed tomography (CT), and ultrasound (sonography), allow for non-invasive longitudinal imaging of disease progression and compound biodistribution.[(p1),(p2)]

For example, preclinical PET allows for quantitative imaging of radiolabeled compounds with the aim to assess the absorption, distribution, metabolism, and excretion (ADME) profiles of drug candidates and to determine drug–target engagement, with resolution of ~1–5 mm; thus, it is best suited for studying macroscopic changes.[(p3),(p4)] The use of radiolabeled compounds is complex and can limit the utility of PET in specific research settings. One of the key applications of MRI in pharmacological research is characterizing drug-induced changes in tissue morphology for evaluating drug toxicity and treatment response. Functional MRI is applicable for detecting blood oxygen level-dependent contrast changes to map blood flow and brain activation patterns in response to drug treatment. The resolution of MRI has traditionally been at the mil-

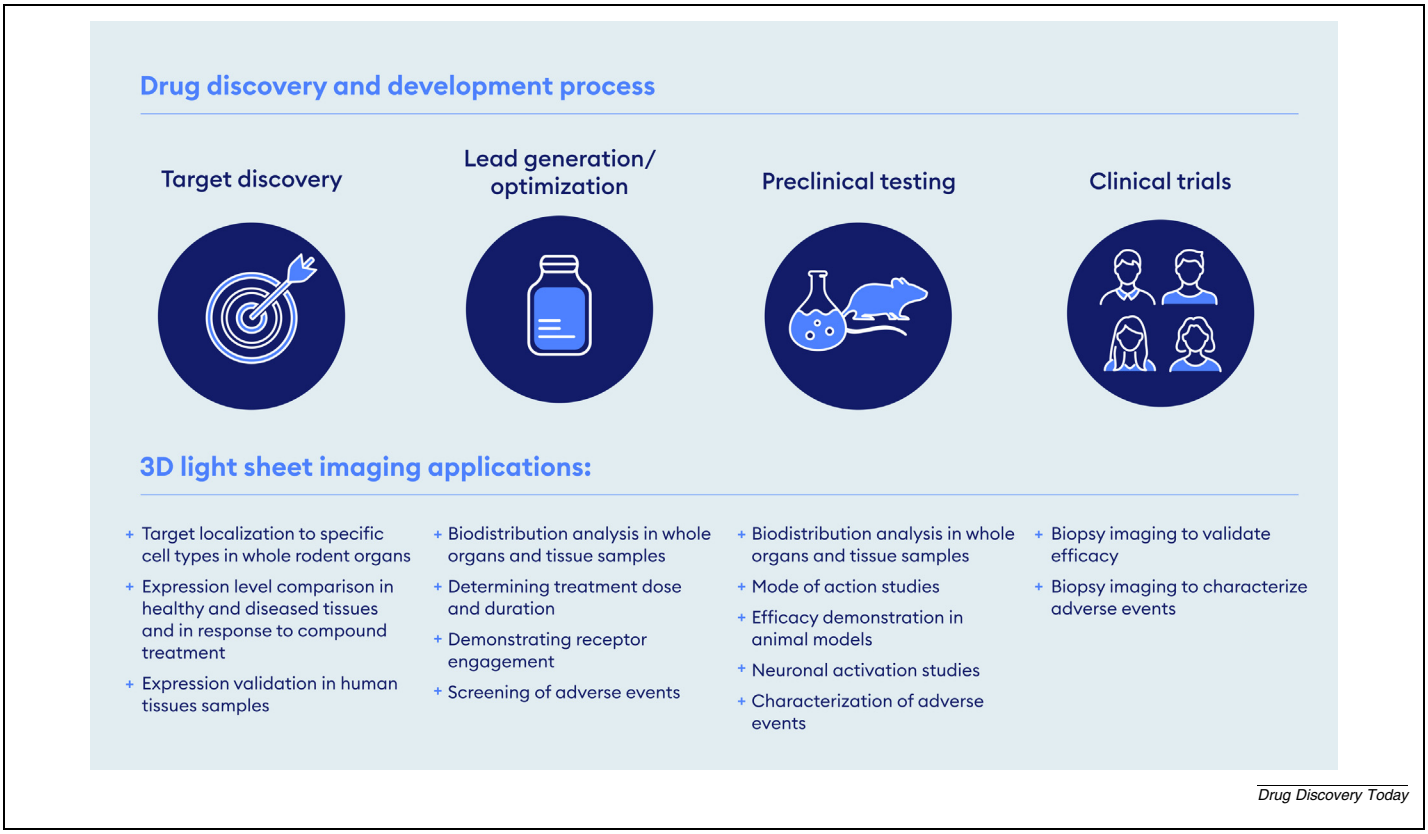

FIGURE 1

Overview of the main applications of 3D light sheet fluorescence microscopy (LSFM) in different phases of drug discovery and development. In early target discovery, LSFM can be applied to visualize target protein or mRNA distribution in both rodent organs and human tissue samples. Expression level can be compared between healthy tissue and in diseases. It can be used to visualize to what extent the target gene expression responds to treatment with known pharmaceuticals. The biodistribution of the lead compound can subsequently be visualized to characterize on– and off-target localization in tissues to identify the best compound for further development. In this phase, imaging can also assist in determining optimal treatment dose and duration and demonstrating receptor engagement. In the subsequent preclinical phase, 3D imaging is often applied in mode-of-action studies and in studies characterizing neuronal activation and drug efficacy in disease models. In eventual clinical trials, biopsies could be imaged in 3D to demonstrate efficacy and adverse events.

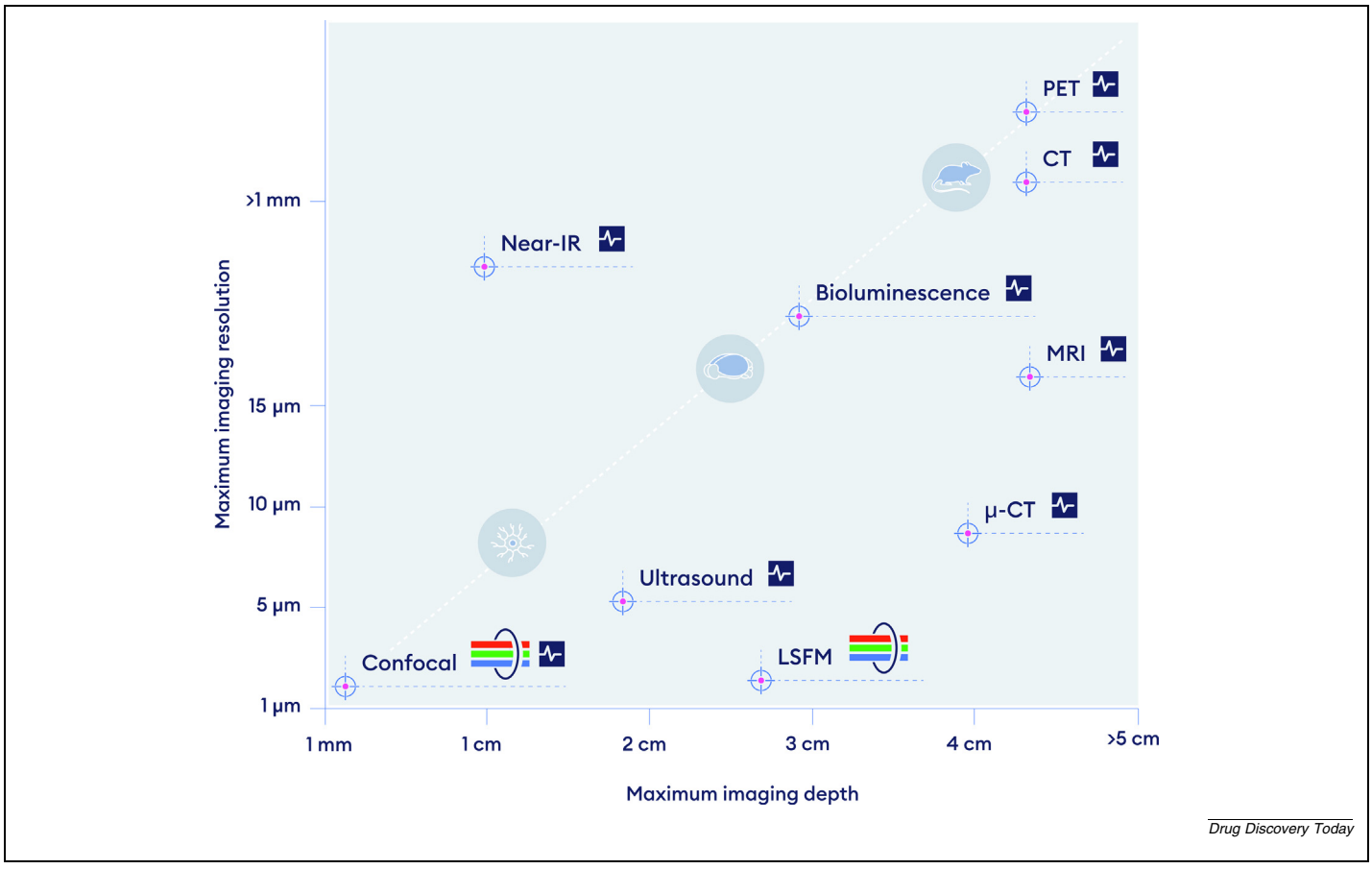

FIGURE 2

Maximum resolution and imaging depth for common preclinical imaging modalities. Multicolor-capable imaging modalities are indicated with an icon of red–green–blue wavelengths (lines) passing a lens, and *in vivo*-capable imaging modalities with heartbeat symbol next to them. Abbreviations: μ-CT, micro-computed tomography; IR, infrared; LSFM, light sheet fluorescence microscopy; MRI, magnetic resonance imaging; PET, positron emission tomography.

limeter scale, but recent technological advances allow for detecting tissue structures down to 15 μm.[(p5),(p6)] 3D ultrasound localization microscopy technology enables imaging of blood flow in vasculature at a resolution down to 5 μm and has proven instrumental in the characterization of mouse models of stroke and visualizing central nervous system (CNS) activation signatures in response to diverse stimuli.[(p7)] The applicability of whole-organism bioluminescence imaging has been increased by the development of brighter compounds and more sensitive systems to enable detection of a few emitting cells in living animals, with spatial resolution usually limited to millimetres.[(p8)] Near-infrared (NIR) imaging is commonly used to study compound biodistribution or to monitor the expansion of fluorescent tumors. In most common settings, the resolution is limited to ~100 μm with an imaging depth of ~0.4–1 cm, with recent advances aimed at improving imaging depth.[(p9),(p10)] Both NIR and bioluminescence imaging rely on the use of viral vectors or transgenic animals which limits their applicability in pharmacological studies. Last, CT is often applied to provide a 3D overview of dense tissues, including bones and solid tumors. The resolution of *in vivo* micro-CT can be down to a few hundred micrometers, whereas *ex vivo* (and some *in vivo*) micro-CT methods can resolve details in the range of few micrometers.

All in all, while the above imaging modalities offer excellent opportunities to characterize morphological changes over time, they typically lack the level of resolution required to distinguish individual cells. Furthermore, the signal, being radioactive, fluorescent, or contrast based, is usually captured alone and without the possibility of adding cell- or tissue-specific markers. Although confocal microscopy and multiphoton microscopy can be used to image different wavelengths, these systems are not well suited for large samples. All these limitations can be overcome using 3D LSFM, whereby multiple fluorescent markers can be imaged simultaneously in the entire organ at single cell resolution.

Sample preparation for LSFM

A rapidly expanding number of methods have been established, enabling quantitative LSFM analysis of diverse tissue types, disease models, and markers. Here, we focus on the application of LSFM in large, cleared tissue samples, but the microscopy technology itself is also applicable to smaller living organisms and organoids. The chemical and experimental principles of tissue clearing have been reviewed elsewhere.[(p11),(p12)] Here, we focus on how LSFM can be successfully integrated in the target and drug discovery workflow and describe a range of possibilities offered by the current LSFM methods.

Incorporation of tissue clearing and LSFM in preclinical target and drug discovery usually starts by considering how the samples can be collected. The preparation of intact rodent organs for LSFM necessitates uniform and complete fixation and is commonly achieved by intracardiac perfusion fixation. This approach becomes impractical for large animal models and clinical biopsies, in which immersion fixation can provide good results with some modifications in downstream sample processing.[p13],[p14] The above methods are largely identical to the standard sample collection workflow in histology and pathology laboratories, which simplifies the implementation of LSFM. Whole-organ imaging methods have been established with the aim to detect proteins, mRNAs, and diverse fluorophore-conjugated drugs. Immunohistochemistry protocols using primary and secondary antibodies allow for detecting cells of interest, changes in signaling pathways, and localization of drug targets. To facilitate sufficient antibody penetration throughout the large tissue volume, the protocols involve different chemical steps to remove lipids and loosen the extracellular matrix. For mouse organs, immunohistochemistry and clearing protocols have been optimized for the brain,[p15],[p16],[p17] kidney,[p18],[p19] bone samples,[p20],[p21],[p22],[p23] heart,[p24],[p25] adipose tissue,[p26] and eye,[p27] as well as for the entire mouse.[p28],[p29] In addition, protocols are available for human organs and tissue samples.[p13],[p14],[p30],[p31] Fluorescent proteins, expressed in transgenic animal models or by viral vectors, can be detected with suitable antibodies (i.e., anti-GFP) or imaged directly by selecting suitable clearing methods that preserve the signal.[p32],[p33],[p34],[p35] Recent advancements in the field have demonstrated high-resolution 3D gene expression analysis by multiplex mRNA *in situ* hybridization (ISH) in tumor samples[p36] and intact mouse brain.[p37],[p38]

Whole-organ LSFM is only made possible by progress in tissue-clearing methods. In simple terms, tissue clearing typically relies on the transfer of the sample to a refractive index matching solution (Figure 4a–e). In this way, by eliminating refraction and reflection of the illuminating laser beam, the fluorescent signal can be visualized even centimeters deep in the tissue. The basic principle of LSFM relies on shining a thin laser light sheet (with a thickness usually in the range of 3–10 μm) at a specified excitation wavelength on the sample. The images are then captured using an objective positioned either below or above the sample. The sample or the light sheet are then moved axially up or down by the desired step size (commonly 3–20 μm) and the image capture is repeated. The sample can be imaged at each plane at multiple wavelengths. LSFM also benefits from fast acquisition speeds, with each plane imaged in a millisecond timeframe, thereby enabling rapid acquisition of entire organs.

LSFM in drug target discovery

Drug targets are often identified through high-throughput 'omics studies and *in vitro* screens, which provide limited information about drug target distribution across different cell types at the whole-organ level. To ensure that a drug specifically targets a particular cell population, it is crucial to acquire an in-depth understanding of target gene expression patterns in various organs. Whole-organ ISH with LSFM offers an unbiased and rapid method for assessing gene expression throughout entire organs (Figure 4f, g). This technique, which uses DNA probes that can be designed for any transcript regardless of species, circumvents the challenges associated with the development of specific antibodies. Nevertheless, if suitable validated antibodies exist, these can be equally instrumental for evaluating and validating the localization of corresponding target proteins. For example, the glucagon-like peptide 1 receptor (GLP-1R) has emerged as a key target in the treatment of obesity. Using LSFM, the expression of GLP-1R was visualized and mapped in the mouse brain, alongside with a fluorophore-conjugated GLP-1R agonist peptide, to demonstrate target localization and compound distribution.[p39] Polymorphisms in leptin receptor (*LEPR*) and pro-opiomelanocortin (*POMC*) are associated with childhood obesity, raising interest in these proteins in drug discovery. Using transgenic reporter mice, two distinct population of neurons, *Pomc*$^{+}$-*Glp1r*$^{+}$ and *Pomc*$^{+}$*Lepr*$^{+}$ were identified in the hypothalamus, with distinct functions in the regulation of food intake.[p40] In a similar manner, using whole-brain imaging, melanocortin-3 receptor (*Mc3r*) was found to be primarily expressed in hypothalamic brain regions known to have a role in food intake, and supporting the development of pharmaceuticals targeting MC3R for the treatment of anorexia.[p41]

Pathological accumulation of alpha-synuclein (α-Syn) is a hallmark in a subset of neurodegenerative disorders and dementias, commonly referred to as α-synucleinopathies. LSFM of the intact mouse brain offers unique advantages to study these diseases because it enables precise 3D mapping and quantification of α-Syn spreading, including in the α-Syn seeding model established by intracerebral injection of preformed fibrils (PFFs). LSFM in combination with available brain-wide anatomical connectivity data has been instrumental to map and predict longitudinal changes in pathological α-Syn spreading in the mouse PFF model, opening possibilities to use the method for identifying drug interventions that could halt or reverse α-synucleinopathy.[p42] Similarly, Alzheimer's disease (AD) represents the most common form of dementia and is characterized by progressive memory loss. Accumulation of β-amyloid peptide (Aβ) and its aggregation into amyloid plaques together with progressive deposition of intracellular hyperphosphorylated tau protein represent the histopathological hallmarks of the disease, resulting in neuronal death. Using a plaque-specific dye (Congo Red), the accumulation of Aβ plaques has been characterized by LSFM in a standard mouse model of AD at different stages of disease progression.[p43] We anticipate that 3D LSFM whole-brain imaging in AD mouse models will help identify drug candidates with improved CNS accessibility and therapeutic efficacy in AD.

LSFM is also applicable in the context of infectious diseases. Severe acute respiratory syndrome coronavirus 2 (SARS CoV 2) enters cells by binding to angiotensin-converting enzyme (ACE)-2, following which the spike protein is cleaved by the transmembrane serine protease 2 (TMPRSS2) to facilitate viral–host membrane fusion. By LSFM mapping the localization of these membrane proteins in healthy and diseased hamster lungs,

it was concluded that the infection occurred in tertiary bronchi, bronchioles, and alveoli, where both proteins were present, and not in other areas of the lung, where only one or the other was detected.[p44] These studies provide examples of how the distribution of drug targets can be characterized in 3D at the whole-organ level. This information is often important in the drug design process, which needs to consider how the specific cell populations can be reached with treatment.

Drug biodistribution assessment in cleared organs

Imaging drug distribution in model organisms is a fundamental part of preclinical drug development. It is important in determining that the drug specifically reaches the specific cell population or molecular target (target engagement), testing different delivery routes, establishing PK and pharmacodynamic (PD) parameters and in understanding how each of these parameters can influence the choice of drug dose in efficacy studies. From a 3D imaging perspective, drug biodistribution studies represent in many ways the simplest study design, where a fluorophore-conjugated compound is administrated in a single or multiple dosing regimen, followed by rapid organ clearing, LSFM scanning, and quantification of the fluorescent signal as a proxy for compound distribution.

Several studies have focused on characterizing the distribution of GLP-1R agonists in the brain, because central action is essential for the weight-lowering properties of this drug class. Using whole-brain LSFM in mice acutely dosed with the fluorophore-conjugated GLP-1R agonist liraglutide, it was demonstrated that the compound largely accumulating in the circumventricular organs [CVOs; i.e., area postrema (AP), median eminence, vascular organ of the lamina terminalis, subfornical organ], but was also detected in a few brain regions beyond the blood–brain barrier (primarily in the arcuate nucleus of the hypothalamus, ARH).[p45],[p46] In a subsequent LSFM study, liraglutide and semaglutide, a GLP-1R agonist with longer half-life, were found to show some differences in signal distribution in the brain, which could explain the differential efficacy on weight loss of these two compounds.[p39] By also performing the experiment in *Glp1r*-knockout mice, GLP1R-dependent accumulation of these two compounds in specific brain regions was validated.[p39] Further comparative quantitative whole-brain analysis of lipidated GLP-1R agonists has supported the benefits of peptide lipidation in gaining CNS access.[p47]

Therapeutic antibodies hold great promise for the treatment of a variety of diseases and the field is developing at a fast pace. The delivery and distribution of antibodies can be analyzed by 3D LSFM using either direct conjugation to a fluorophore or a fluorescent secondary antibody. As an example, dosing of tumor-bearing mice with fluorescent therapeutic antibodies directed against human carbonic anhydrase XII (CA XII) facilitated imaging of targeting efficacy in metastases. The results indicated that the therapeutic antibody efficiently targeted the primary tumor and metastases in the lungs, but had lower efficiency in reaching metastases in the rest of the body.[p48] Epithelial cell adhesion molecule (EpCAM) represents historically one of the first and most studied cancer-associated biomarkers and drug targets. Given that the gene is also expressed in healthy epithelial cells across diverse organs, a balance needs to be achieved to assure sufficient targeting of tumor cells. Using 3D imaging of entire cleared mice as well as isolated organs in higher detail enabled studying the distribution of intravenously dosed fluorophore conjugated anti-mouse EpCAM antibodies.[p49]

Compared with therapeutic antibodies and peptide drugs, the biodistribution of small molecules has been difficult to image because of challenges in fluorescent labeling while preserving functionality and achieving reliable drug–tissue fixation. To overcome the first obstacle, CLICK chemistry has been applied to visualize small molecules covalently bound to drug targets. For this purpose, alkyne handle-conjugated drugs were made visible by subsequent addition of azide-Alexa647 with a CLICK reaction in the intact tissue. This enabled quantitative 3D visualization of drug–target engagement for fatty acid amide hydrolase inhibitors as well as for a monoamine oxidase inhibitor in the mouse brain.[p50] To overcome the second challenge in visualizing small molecules that do not covalently bind the receptor, a strategy was developed in which a primary amine was added to the target molecule, enabling it to be fixed by formaldehyde to the surrounding proteins. Using this approach, several small molecules, including spiperone, an antipsychotic schizophrenia drug, were imaged in whole-mouse brain.[p51] These studies have set the groundwork for future small-molecule biodistribution studies using 3D LSFM imaging.

Adeno-associated viruses (AAV) constitute the bulk of gene therapies. Evaluating which of these viral vectors target the intended cells is crucial for ensuring treatment efficacy and minimizing potential side effects (Figure 4h). Accordingly, 3D LSFM imaging was used to compare the transduction efficiency of different recombinant AAV serotypes dosed intramuscularly to identify those capable of reaching the spinal cord and brainstem.[p52] LSFM was also applied to image efficient AAV transduction of neurons following an intracerebral stereotactic AAV injection in a Huntington's disease model, with further molecular analyses confirming its gene-editing efficiency.[p53] Given that the gene therapy field is still at an early stage, the number of studies focused on validating novel therapeutic vectors in disease models will likely increase. The same holds true for therapeutic stem cells. Following systemic or local delivery into the tissue, the fate of the cells is often difficult to assess because of their low survival probability and spread across large tissue regions. The transplanted cells can be detected either by imaging fluorescent protein expression or by detecting human stem cells in mice by staining for anti-human IgG antibodies.[p54]

CNS mode of action studies

LSFM has gained increasing popularity in preclinical mode-of-action (MoA) studies, in particular within the field of neuroscience. The mammalian brain displays a highly organized structure with minimal variation between individuals. A mouse brain comprises >1000 brain regions, with many of them having well-characterized functions established in basic neuroscience experiments and supported by clinical data. The 3D coordinates of each brain region have been established in the average mouse brain atlas (the *Allen Reference Atlas*) using two-photon tomography images.[p55] Automated mapping of

LSFM data to the brain atlas space provides a unique opportunity to characterize neuronal activation signatures across the brain and within specific brain regions. *C-fos* is a proto-oncogene that is expressed within many neurons following depolarization and, thus, is considered a proxy for neuronal activity (Figure 4i). In a pioneering study, Renier *et al*. applied whole-brain 3D LSFM c-Fos imaging to characterize neuronal activation patterns in response to behavioral stimuli, laying the groundwork for automated c-Fos mapping, quantification, and visualization.[p56] This approach has subsequently been applied in numerous pharmacological studies in mice.

For example, several studies have mapped c-Fos activation signatures of weight-loss drugs. The neural circuits regulating appetite and food intake are generally well characterized. In brief, homeostatic control of appetite involves peripheral signals (hormones) reaching the AP, nucleus of the solitary tract (NTS), and the ARH, which are connected to deeper brain regions in the hypothalamus, amygdala, and parabrachial nucleus. Nonhomeostatic (hedonic) regulation of appetite includes many of the above brain regions with distinct activated neuronal populations, but also recruits reward-related signaling originating from the midbrain, notably the ventral tegmental area.[p57] c-Fos imaging and quantification following acute administration of semaglutide or liraglutide revealed an increase in c-Fos-positive cells primarily in brainstem nuclei (AP and NTS), parabrachial nucleus, hypothalamus (ARH and parasubthalamic nucleus), central nucleus of the amygdala, and bed nuclei of the stria terminalis. Comparison of the c-Fos response to the biodistribution of the corresponding fluorescent-tagged compounds revealed a partial overlap between drug accumulation and c-Fos response primarily in the brainstem, enabling the authors to conclude that the compounds indirectly activate deeper-lying brain regions, which may be important for the appetite-suppressive effects of this drug class.[p39],[p46],[p58] These studies support the notion that the parabrachial nucleus is a key relay for signals originating from the AP and NTS, and subsequently further transmitted to canonical mid- and forebrain regions regulating body-weight homeostasis.[p39],[p58] Comparison of c-Fos signatures of the weight-lowering compounds semaglutide, bromocriptine, rimonabant, lorcaserin, and setmelanotide revealed an overlapping c-Fos activation pattern in brain regions with established roles in body weight and satiety regulation, in particular in the brainstem, amygdala, and hypothalamus [p59] The results also highlighted key differences between the individual MoA of the drugs. Interestingly, semaglutide resulted in a highly discrete brain regional activation pattern, reflecting predominantly CVO-restricted accumulation of the drug, while all other weight-loss compounds promoted brain-wide activation. Some of the observed neuronal activation signatures can help explain the adverse events observed for these drugs, exemplified for rimonabant by increased c-Fos activity in the prefrontal cortex and amygdala.[p59]

Considering the successful clinical development of GLP-1R agonists for obesity, significant efforts have been made to identify drug targets that can potentiate GLP-1R agonist-induced weight loss to a magnitude that presently can only be achieved by gastric bypass surgery. Tirzepatide represents a benchmark peptide pharmaceutical, targeting both GLP-1R and gastric inhibitory polypeptide receptor (GIPR) and demonstrating the benefits of dual agonists.[p60] Whole-brain 3D imaging can be instrumental in characterizing drug combinations that can have complimentary brain activation signatures to promote additive effects on weight loss. Using whole-brain LSFM imaging, co-activation of GLP-1R with either nicotinic acetylcholine receptors or neuropeptide Y receptor type 2 was found to enhance c-Fos activation in key appetite-regulating regions, resulting in greater body-weight loss compared with monotherapies.[p61],[p62] Similarly, preclinical evidence has shown the benefits of small-molecule NMDA receptor antagonists in suppressing food intake, but clinical translation has been prevented by severe adverse events. Conjugating the N-methyl-D-aspartate (NMDA) receptor antagonist MK-801 to a GLP-1 analog enabled targeting of the effect to GLP-1R-expressing cells, resulting in an improved safety profile and body-weight loss. Using LSFM of c-Fos-positive neurons indicated that GLP-1–MK-801 treatment increased neuronal activation in some amygdala and midbrain regions compared with semaglutide.[p63]

The development of more effective therapeutics for depression and other psychiatric disorders has remained challenging. One reason for this is the lack of understanding of underlying disease mechanisms. Almost all psychiatric disorders affect multiple brain regions, making it difficult to characterize druggable pathways and the MoAs of therapeutics. An historical research focus on specific cell populations in defined brain regions has hindered our understanding of neuronal signaling in psychiatric disorders. Whole-brain 3D imaging can bring a change to the drug discovery process for psychiatric disorders because it helps unbiased mapping of neuronal activation across the brain. Furthermore, the neuronal activation information can be combined with LSFM experiments to visualize connectivity between brain regions (i.e., by viral tracing), helping to generate a better understanding of the interplay between the different activated cell populations. Given that most existing antipsychotic drugs represent small molecules, progress in establishing methods for the

FIGURE 3

Overview of possible applications for light sheet fluorescence microscopy (LSFM) in organ-specific drug efficacy studies. In oncology, imaging can be used to visualize tumor growth, metastases,[p29],[p93],[p96] cell proliferation,[p74],[p94] inflammation[p75] and vascular changes.[p73] In renal disease research, LSFM can be used to count and analyze glomeruli,[p19],[p76],[p77] inflammation[p79] vascular changes,[p80] kidney tubules,[p78] innervation,[p18] and changes in podocyte numbers and morphology. In women's health and fertility research, imaging can count oocytes and analyze ovarian follicle maturation.[p84] In male fertility, the morphology of seminiferous tubules can be characterized.[p85] In digestive system disorders, the morphology of intestinal surface can be visualized,[p86] and enteric innervation[p28] and microbial distribution[p87] can be quantified. For skeletal muscle diseases, the overall morphology, patterning, and size of muscles can be assessed[p31],[p89] and neuromuscular junctions quantified.[p89] In the adipose tissue, the total number of adipocytes, their volume and inflammation can be assessed.[p26],[p88] In diabetes research, the islet count, and volume can be quantified in the entire pancreas, the β cell mass analyzed, β cell proliferation assessed, and inflammation quantified in type 1 diabetes mellitus.[p13],[p81],[p82] In brain research, tyrosine hydroxylase-positive neurons can be quantified in Parkinson's disease models,[p97] Alzheimer's plaques counted and their size analysed,[p43],[p67] microglia quantified,[p43] and neuronal activation analyzed in response to physiological and pharmacological stimuli, including for anti-obesity pharmaceuticals.[p56],[p59] In eye disease, the morphological changes in the outer nuclear layer can be assessed, photoreceptors quantified, and vascular changes assessed.[p70],[p98],[p99] In lung diseases, the airways and immune cells can be visualized and quantified per lung lobe.[p83] In cardiovascular biology, the capillary density can be assessed in disease models, morphological changes and infarction extent analyzed, and inflammation visualized.[p24],[p25] The atherosclerotic plaques and plaque content can be quantified in the aorta and arteries.[p71],[p72]

visualization of small-molecule receptor engagement and distribution in the brain will help in future drug development work.[p50],[p51]

LSFM has so far only been used in few studies on drugs relevant to psychiatric disorders. Whole-brain imaging was used to study the mechanisms of psilocybin action, a naturally occurring psychedelic and preferential 5-$HT_{1A/2A}$ agonist with anti-depressive efficacy. LSFM data indicated that psilocybin treatment resulted in an increase in the number of c-Fos-positive cells in a large part of neocortex, spanning somatosensory, motor, visceral, auditory, gustatory, agranular insular, and temporal regions.[p64],[p65] Antipsychotic drugs are associated with adverse metabolic effects, notably obesity and diabetes. Conceptually, developing novel therapeutics with preferential action in brain regions related to the psychiatric disorder, but at the same time modulating the activity in appetite-regulating regions, could therefore be beneficial in the development of next-generation antipsychotics. As an example of this

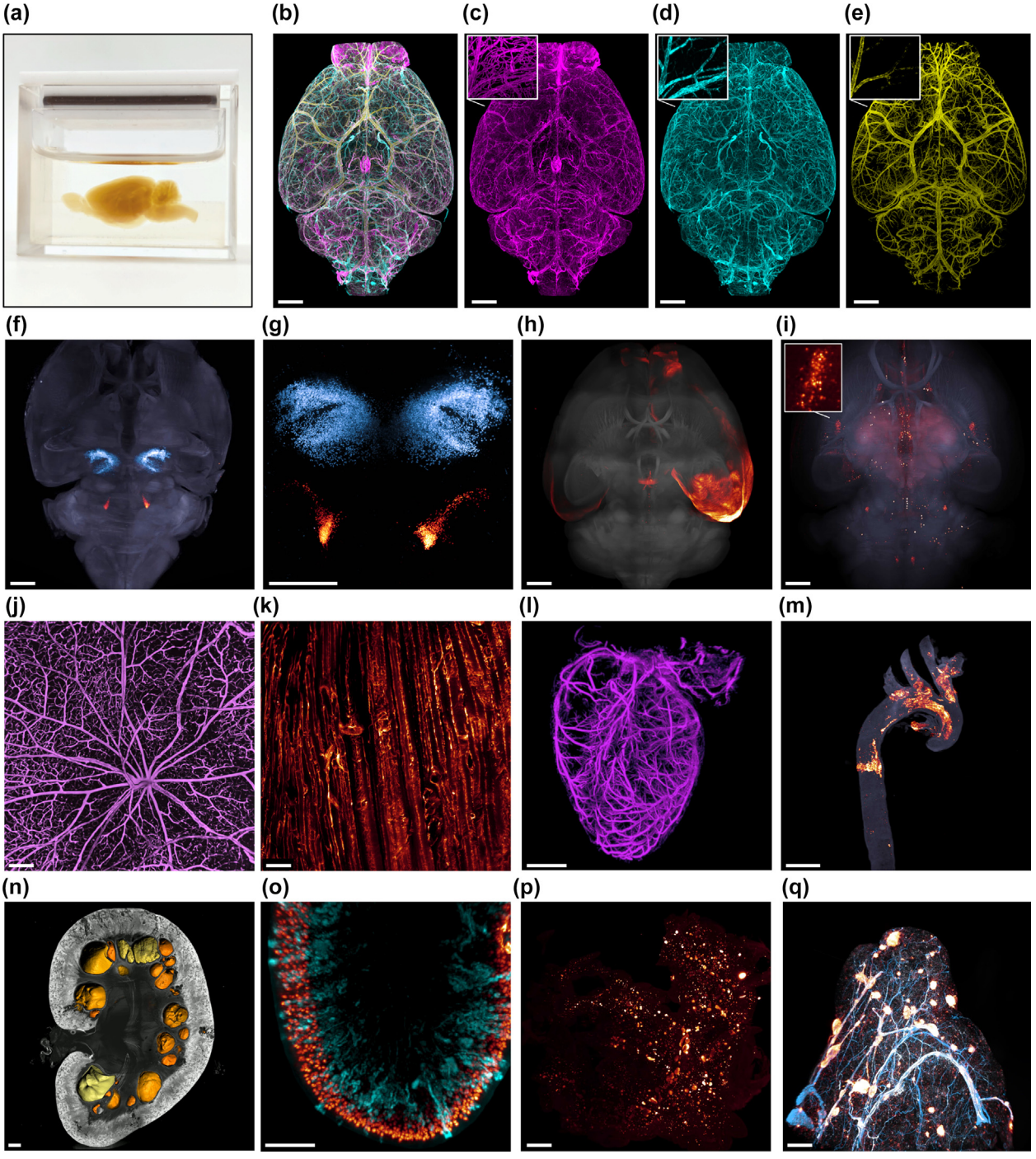

Drug Discovery Today

approach, trace amine-associated receptor 1 (TAAR1) agonists, which are in clinical development for depression, anxiety, and addiction, have recently been characterized by LSFM, which indicated potent activation of brain regions regulating both mood and food intake, with considerable overlap with regions well known to be activated by GLP-1R agonists (see above).[p66]

Disease pathology and drug efficacy characterization

Whole-organ imaging provides a unique opportunity to characterize animal models of human diseases and quantify preclinical drug efficacy. LSFM can be instrumental for demonstrating changes in disease-associated cell populations (i.e., leukocytes and fibroblasts), characterizing up- or downregulation of cellular signaling pathways, and visualizing morphological changes in the tissue. Overall, LSFM is highly customizable to visualizing and quantifying endpoints relevant to diverse diseases and drug classes (Figure 3).

As an example of applying LSFM in neurodegenerative diseases, a mouse model of AD was treated with either the β-secretase 1 inhibitor NB360, an antibody targeting αβ, or the amyloid-binding small molecule LIN5044. The brains were stained with fluorescent dyes (polythiophenes qFTAA and hFTAA), distinguishing plaques in early development and older plaques. This method permitted accurate assessment of total plaque numbers, volume, and maturation following mapping to a reference brain atlas. Although the study demonstrated limited efficacy of the αβ antibody, a strong beneficial effect was seen for both NB360 and LIN5044. Intriguingly, whole-brain analysis demonstrated largely divergent effects of these compounds on AD pathology. LIN5044 was primarily effective in rostrodorsal parts of the brain and in reducing the growth of existing plaques, whereas NB360 was effective in the ventrocaudal aspects of the brain, affecting plaque formation in young mice, with limited effect on their subsequent growth. These data provide a better understanding of the different effects of therapeutics on primary and secondary plaque nucleation and growth, and help to design clinical trials and interpret the resulting data.[p67] A LSFM pipeline has also been established for key Parkinson's disease endpoints, quantifying brain-wide tyrosine hydroxylase expression and neuronal counts in the affected midbrain regions,[p68] which will enable testing of novel drug candidates targeting the dopaminergic system.

3D LSFM is particularly powerful in the analysis of vasculature because the complex capillary network is difficult to capture on 2D histological sections (Figure 4j, k). Vascular pathology is common across a large variety of diseases and, thus, the methodology has broad applicability. With LSFM of cleared samples, one can capture several parameters, including vascular branch point density, regional changes in vascular diameter, and stochastic vascular malformations.[p69] LSFM was applied for quantification of vascular pathology in an oxygen-induced retinopathy mouse model, commonly used to study the vascular changes arising in diabetic retinopathy. Compared with vehicle-dosed controls, 3D eye scans from mice treated with everolimus (an mTor inhibitor) demonstrated a reduction in vascular tuft volume and improved tuft morphology, providing mechanistic insight into the MoA of the drug.[p70] Capillary rarefaction manifests in myocardial infarction and accompanies tissue fibrosis, resulting in loss of myocardial contractility. 3D imaging has been established for precise analysis of avascular area and capillary rarefaction in a left descending coronary artery ligation mouse model of myocardial infarction.[p24],[p25] Spatial segmentation of the infarcted heart into infarct zone, border area, and healthy myocardium in parallel with capillary density analysis demonstrated an effect of the ACE inhibitor captopril on vascular density in the border zone.[p25] LSFM can also be applied to large blood vessel analysis (Figure 4l, m) and has been used to quantify atherosclerotic plaques in the aorta and its arterial branches.[p71],[p72]

LSFM is ideally suited for oncology research. Tumor metastasis is highly variable, making it challenging to analyze using conventional histology, whereas standard whole-body imaging modalities lack sufficient resolution to detect small metastases. With LSFM, one can rapidly image organs or, at a lower throughput, even the entire mouse to detect tumor metastasis and delineate desired intratumor therapeutic targets. For example, blood vessel development in tumors has been an active drug target and anti-angiogenic therapies are used for blunting tumor

FIGURE 4

Examples of light sheet fluorescence microscopy (LSFM) application in diverse organs and disease models. **(a)** Intact rat brain, cleared in ethyl cinnamate and positioned in customized quartz cuvette, ready for imaging using a Bruker Luxendo LCS SPIM microscope. **(b)** Intact cleared mouse brain stained with antibodies against endothelial marker CD31 (magenta), venous vasculature-enriched Von Willebrand factor (cyan), and arterial smooth muscle marker transgelin/SM22a (yellow). **(c–e)** Individual channels of the image in (b) shown separately. Same area is magnified on a 2D digital plane in the top-left corner. **(f)** Mouse whole-brain mRNA *in situ* hybridization, mapping the expression of the dopamine transporter (DAT) gene *(Slc6a3)* in blue and the norepinephrine transporter (NET) gene (*Slc6a2*) in glow. Brain background fluorescence is shown in gray. **(g)** Substantia nigra (DAT expression) and locus coeruleus (NET expression) of the brain in (f) magnified to demonstrate the single cell resolution of mRNA imaging. **(h)** LSFM imaging of mouse brain stained for GFP (in glow) 2 weeks following stereotactic dosing of AAV9-CAG-GFP virus into the entorhinal cortex. **(i)** LSFM imaging of mouse brain stained for c-Fos (in glow, marker of neuronal activation), as determined 2 h after single dosing with semaglutide, a glucagon-like peptide-1 (GLP-1) receptor agonist**.** The amygdala region is magnified in the box**.** Brain background fluorescence is shown in gray. **(j)** Visualization of mouse retina stained for CD31. **(k)** Mouse soleus muscle, where capillary blood vessels are visualized following *in vivo* dosing of DyLight 649-labeled tomato lectin. **(l)** Transgelin (SM22a) immunohistochemistry in intact mouse heart. **(m)** Visualization of immune cell infiltrates (CD45 immunohistochemistry, glow) within aortic atherosclerotic plaques in a diet-induced obese mouse dosed with AAV encoding for proprotein convertase subtilisin/kexin type 9 (PCSK9-AAV). **(n)** LSFM imaging applied to a rat model of polycystic kidney disease. The kidney was imaged in autofluorescence wavelength and cysts (yellow) were detected by computational image analysis. **(o)** Visualization of podocin (glow) and kidney injury molecule 1 (KIM1, cyan) immunohistochemistry in a ReninAAV-UNx db/db mouse model of hypertensive diabetic kidney disease. **(p)** 3D visualization of insulin-labeled islets in the entire healthy mouse pancreas. **(q)** Visualization of inflammation (CD45, glow) and vascular smooth muscle (transgelin, blue) in white adipose tissue samples from a diet-induced obese mouse model of metabolic dysfunction-associated steatohepatitis. Scale bars: 1 mm (b–i, l–p) and 100 μm (j,k).

growth. LSFM imaging revealed how axitinib/gemcitabine cotreatment reduced the number of small-diameter vessels and vessel branching in tumors without affecting overall vascular density in a medulloblastoma model.[p73] Inhibition of cancer cell proliferation by therapeutics could also lead to tumor shrinkage. An interesting approach to study cell proliferation in 3D is by transplanting mice with cancer cells expressing a fluorescent cell cycle indicator (Fucci). The Fucci lentiviral vector results in cells expressing GFP in M and G2 phase and red fluorescent protein (RFP) in G1 phase. LSFM of mice treated with a 5-fluorouracil cell cycle inhibitor showed a marked shift from red fluorescent tumors to green fluorescent tumors, indicating G2/M arrest, before resulting in cell death and tumor shrinkage.[p74] Current drug discovery efforts in oncology are often focused on modulating the immune response to the tumors. Whole-organ imaging is beneficial for detecting immune cell subsets in large tissue volumes and assessing the treatment response. Using fluorescent nanoparticles, tumor-associated macrophages were visualized in lung cancer mouse models and the effect of Pexidartinib (PLX3397), a tyrosine kinase inhibitors of CSF-1R (Colony stimulating factor 1 receptor) on reducing the density of the macrophages was shown.[p75]

With tissue clearing and LSFM, it is possible to image entire rodent kidneys and map pathological changes in every glomerulus and in the vasculature at the capillary level, plus studying the different segments of the kidney tubules (Figure 4n, o). In a nephrotoxic nephritis mouse model of human crescentic glomerulonephritis, LSFM indicated a spatially patchy pathology with a reduction in glomerular count at 2 weeks following disease induction. The loss of approximately one-third of glomeruli was particularly evident in glomeruli with small- and medium-sized tufts and was associated with an increase in the albumin: creatine ratio.[p19] In the context of diabetic nephropathy, using uninephrectomized (UNx) db/db mice, an increase in mean glomerular volume was detected, whereas the total number of glomeruli did not change.[p76] In a relatively more advanced model of hypertensive diabetic kidney disease (ReninAAV UNx-db/db mice), LSFM was applied to demonstrate the effect of cotreatment with an angiotensin I converting enzyme (ACE) inhibitor (lisinopril) and a sodium/glucose cotransporter 2 (SGLT-2) inhibitor (empagliflozin) on reducing glomerular hypertrophy.[p77] 3D imaging has also been used to characterize pathological changes in kidney innervation following acute ischemia reperfusion injury, showing that nearly 70% of the sympathetic nerves are lost.[p18] In addition, the length of tubular segments can also be visualized and quantified in cleared kidneys[p78] as well as accumulation of immune cells.[p79] Last, imaging has been implemented to demonstrate loss of peritubular capillaries and reduction in vascular branching in mouse model of chronic tubulointerstitial nephritis.[p80]

Similarly to kidney glomeruli, LSFM can be applied to detect all pancreatic islets and quantify the total insulin-producing β cell volume in healthy and diabetes mouse models (Figure 4p).[p81],[p82] Dosing of mice with the insulin receptor antagonist S961 resulted in an overall increase in islet number and size as well as cell proliferation within islets, indicating the suitability of 3D light sheet imaging for characterizing treatment effects across the entire pancreas.[p82] LSFM was demonstrated equally suitable for detecting immune cell accumulation around and in the islets in a mouse model of type 1 diabetes mellitus (T1DM).[p82] Detailed characterization of a T1DM mouse model illustrated a large reduction in both islet volume and count, affecting in particular the large islets and duodenal lobe, accompanied by increased innervation of remaining islets.[p81] The results suggest reorganization of pancreatic islet innervation in diabetes, which could represent a new therapeutic avenue.[p81]

The application of LSFM is also being evaluated for many other diseases. Imaging of entire lungs at high resolution brings the benefit of detecting sparsely located inflammatory foci and quantifying these in the context of airways in individual pulmonary lobes, for example in asthma models.[p83] LSFM holds also great promise for reproductive organ diseases and drug development for fertility, for which oocyte maturation and count can be quantified in entire ovaries[p84] or tubular morphology analyzed in the testis.[p85] For the digestive system, LSFM has been applied to study enteric innervation, visualize distribution of microbiota, and characterize the morphology of the intestinal surface.[p28],[p86],[p87] Whole-organ imaging can also be valuable for assessing skeletal muscle morphology, distribution of neuromuscular junctions, as well as adipose tissue morphology and inflammation (Figure 4q).[p88],[p89] Overall, imaging the entire organ provides better sensitivity to detect even small treatment effects during the early drug discovery process and could help to select the best drug candidates for further development.

Toward applying LSFM on human samples

There has been consistent interest in imaging tissue samples from clinical biopsies, with several methods optimized for human samples. As an example, LSFM was applied to study the entire human pancreas, showing unexpected heterogeneity in islet composition, with nearly half of islets containing only a few glucagon-producing α-cells.[p13] Similarly, pancreatic islet innervation was characterized using human pancreas tissue samples.[p81] LSFM was also implemented for describing plaque morphology and density in archival brain samples from patients with AD, revealing large amyloid aggregates comparable to those found in standard mouse models of the disease, lending further support to the translatability of these models.[p43] Advances in LSFM and tissue preparation could have a large impact on the analysis of patient biopsies. First, research has focused on providing a 3D imaging alternative to classical histological staining methods. Using staining with fluorescent analogs of Hematoxylin and Eosin together with tissue clearing and LSFM, a rapid pipeline for 3D pathology was established, compatible with diverse healthy and pathological tissue types.[p90],[p91] Similarly, a fluorescent analog for Periodic acid–Schiff (PAS) staining was used to assess the 3D architecture of colonic crypts in inflammatory bowel disease.[p92] LSFM could be particularly valuable in clinical oncology research. Of particular interest is a study

focused on cancer detection in sentinel lymph nodes. These lymph nodes are commonly screened for metastases following removal of the primary tumor and the procedure relies on the assessment of a histological section through the tissue. Head-to-head comparison of standard histology and LSFM in 21 patient samples demonstrated that 3D whole-lymph node LSFM could detect all metastatic lymph nodes that were detected by standard histological methods and could in addition also reveal metastases that remained undetected in histology.[p93] Similar conclusions were drawn in another study on breast cancer samples, 3D imaged for epithelial and cell proliferation markers. The results revealed well-preserved morphology and could detect variability in cell proliferation that was not detectable in standard histology.[p94] Altogether, although 3D immunohistochemistry takes longer, it benefits from higher precision and could in the end have a significant impact on treatment course and the conclusion of drug efficacy.

Concluding remarks and future perspectives

Recent advances in tissue clearing, labeling, and microscopy techniques have significantly improved our ability to image various tissues and detect the distribution of drugs, proteins, and mRNAs. These developments have been accompanied by significant efforts to automate sample handling, increase imaging speed, and improve image analysis workflows. These advancements are set to expand the use of LSFM in preclinical and clinical research and eventually to be implemented in routine pathology workflows. Automated data processing and artificial intelligence (AI)-based analysis workflows are of key significance in the LSFM workflow. Such computational obstacles can remain a significant barrier for smaller research teams without dedicated infrastructure and computational analysis support. Both commercial and open-source platforms that help to make AI-based analysis of large 3D images user-friendly can help break down this barrier.[p95] In the years ahead, LSFM will increasingly offer new opportunities for imaging tissue samples from large animal models and in clinical settings. The scarcity of suitable antibodies has frequently posed challenges for imaging tissues from nonrodent sources. However, recent advancements in mRNA *in situ* hybridization, which allows for the detection of any desired transcript, represents a promising avenue for expanding 3D imaging into various new species and tissue types. The future will likely also see greater interplay between 3D LSFM imaging and diverse spatial biology technologies. Spatial transcriptomics can accurately detect gene expression in selected reference samples, whereas 3D microscopy is scalable to large sample sizes, enabling quantitative pharmacological studies. Overall, we are still in the early phases of using 3D LSFM imaging, a technique that can support many aspects in pharmacological research, from preclinical drug target and drug efficacy studies to evaluating tissue biopsies from patients.

CRediT authorship contribution statement

Urmas Roostalu: Writing – review & editing, Writing – original draft, Visualization. **Henrik H. Hansen:** Writing – review & editing. **Jacob Hecksher-Sørensen:** Writing – review & editing.

Data availability

No data was used for the research described in the article.

Acknowledgments

The authors are grateful to Thomas Topilko, Max Hahn, Yasir Gallero-Salas, Marie Biviano Rosenkilde, Frederikke Lynge Sørensen, Lea Lydolph Larsen, Katrine Skovgård, Sabrina Krarup, and Neringa Zitkute for help with preparing example images. We also thank Louise Munch Blicher for help with graphical design.

References

1. Markicevic M, Savvateev I, Grimm C, Zerbi V. Emerging imaging methods to study whole-brain function in rodent models. *Transl Psychiatry*. 2021;11:457.
2. de Jong M, Essers J, van Weerden WM. Imaging preclinical tumour models: improving translational power. *Nat Rev Cancer*. 2014;14:481–493.
3. Lancelot S, Zimmer L. Small-animal positron emission tomography as a tool for neuropharmacology. *Trends Pharmacol Sci*. 2010;31:411–417.
4. Serkova NJ et al. Preclinical applications of multi-platform imaging in animal models of cancer. *Cancer Res*. 2021;81:1189–1200.
5. Johnson GA et al. Merged magnetic resonance and light sheet microscopy of the whole mouse brain. *PNAS*. 2023;120, e2218617120.
6. Frost GR et al. Hybrid PET/MRI enables high-spatial resolution, quantitative imaging of amyloid plaques in an Alzheimer's disease mouse model. *Sci Rep*. 2020;10:10379.
7. Demeulenaere O et al. In vivo whole brain microvascular imaging in mice using transcranial 3D Ultrasound Localization Microscopy. *EBioMedicine*. 2022;79, 103995.
8. Iwano S et al. Single-cell bioluminescence imaging of deep tissue in freely moving animals. *Science*. 2018;359:935–939.
9. Refaat A et al. In vivo fluorescence imaging: success in preclinical imaging paves the way for clinical applications. *J Nanobiotechnology*. 2022;20:450.
10. Dang X et al. Deep-tissue optical imaging of near cellular-sized features. *Sci Rep*. 2019;9:3873.
11. Ueda HR et al. Tissue clearing and its applications in neuroscience. *Nat Rev Neurosci*. 2020;21:61–79.
12. Tainaka K et al. Chemical landscape for tissue clearing based on hydrophilic reagents. *Cell Rep*. 2018;24:2196–2210.
13. Lehrstrand J, Davies WIL, Hahn M, Korsgren O, Alanentalo T, Ahlgren U. Illuminating the complete ß-cell mass of the human pancreas- signifying a new view on the islets of Langerhans. *Nat Commun*. 2024;15:3318.
14. Zhao S et al. Cellular and molecular probing of intact human organs. *Cell*. 2020;180:796–812.
15. Renier N, Wu Z, Simon DJ, Yang J, Ariel P, Tessier-Lavigne M. iDISCO: a simple, rapid method to immunolabel large tissue samples for volume imaging. *Cell*. 2014;159:896–910.
16. Susaki EA, Tainaka K, Perrin D, Yukinaga H, Kuno A, Ueda HR. Advanced CUBIC protocols for whole-brain and whole-body clearing and imaging. *Nat Protoc*. 2015;10:1709–11027.
17. Ertürk A et al. Three-dimensional imaging of solvent-cleared organs using 3DISCO. *Nat Protoc*. 2012;7:1983–1995.
18. Hasegawa S et al. Comprehensive three-dimensional analysis (CUBIC-kidney) visualizes abnormal renal sympathetic nerves after ischemia/reperfusion injury. *Kidney Int*. 2019;96:129–138.
19. Klingberg A et al. Fully automated evaluation of total glomerular number and capillary tuft size in nephritic kidneys using lightsheet microscopy. *J Am Soc Nephrol*. 2017;28:452–459.
20. Mertens TF et al. MarShie: a clearing protocol for 3D analysis of single cells throughout the bone marrow at subcellular resolution. *Nat Commun*. 2024;15:1764.
21. Jin B-H et al. Optimization of the optical transparency of bones by PACT-based passive tissue clearing. *Exp Mol Med*. 2023;55:2190–21204.

22. Greenbaum A et al. Bone CLARITY: clearing, imaging, and computational analysis of osteoprogenitors within intact bone marrow. *Sci Transl Med*. 2017;9, eaah6518.
23. Nudell V et al. HYBRiD: hydrogel-reinforced DISCO for clearing mammalian bodies. *Nat Methods*. 2022;19:479–485.
24. Merz SF et al. Contemporaneous 3D characterization of acute and chronic myocardial I/R injury and response. *Nat Commun*. 2019;10:1–14.
25. Roostalu U et al. Effect of captopril on post-infarction remodelling visualized by light sheet microscopy and echocardiography. *Sci Rep*. 2021;11:5241.
26. Chi J et al. Three-dimensional adipose tissue imaging reveals regional variation in beige fat biogenesis and PRDM16-dependent sympathetic neurite density. *Cell Metab*. 2018;27:226–236.
27. Henning Y, Osadnik C, Malkemper EP. EyeCi: Optical clearing and imaging of immunolabeled mouse eyes using light-sheet fluorescence microscopy. *Exp Eye Res*. 2019;180:137–145.
28. Mai H et al. Whole-body cellular mapping in mouse using standard IgG antibodies. *Nat Biotechnol*. 2024;42:617–627.
29. Cai R et al. Panoptic imaging of transparent mice reveals whole-body neuronal projections and skull–meninges connections. *Nat Neurosci*. 2019;22:317–327.
30. Belle M et al. Tridimensional visualization and analysis of early human development. *Cell*. 2017;169:161–173.
31. Blain R et al. A tridimensional atlas of the developing human head. *Cell*. 2023;186:5910–5924.
32. Qi Y et al. FDISCO: advanced solvent-based clearing method for imaging whole organs. *Sci Adv*. 2019;5, eaau8355.
33. Hsu C-W et al. EZ Clear for simple, rapid, and robust mouse whole organ clearing. *Elife*. 2022;11, e77419.
34. Pan C et al. Shrinkage-mediated imaging of entire organs and organisms using uDISCO. *Nat Methods*. 2016;13:859–867.
35. Susaki EA et al. Whole-brain imaging with single-cell resolution using chemical cocktails and computational analysis. *Cell*. 2014;157:726–739.
36. Tanaka N et al. Three-dimensional single-cell imaging for the analysis of RNA and protein expression in intact tumour biopsies. *Nat Biomed Eng*. 2020;4:875–888.
37. Kanatani S et al. Whole-brain three-dimensional imaging of RNAs at single-cell resolution. *BioRxiv*. 2022. https://doi.org/10.1101/2022.12.28.521740. Published online December 29, 2022.
38. Murakami TC, Heintz N. Multiplexed and scalable cellular phenotyping toward the standardized three-dimensional human neuroanatomy. *BioRxiv*. 2022. https://doi.org/10.1101/2022.11.23.517711. Published online November 24, 2022.
39. Gabery S et al. Semaglutide lowers body weight in rodents via distributed neural pathways. *JCI Insight*. 2020;5, e133429.
40. Biglari N et al. Functionally distinct POMC-expressing neuron subpopulations in hypothalamus revealed by intersectional targeting. *Nat Neurosci*. 2021;24:913–929.
41. Sweeney P et al. The melanocortin-3 receptor is a pharmacological target for the regulation of anorexia. *Sci Transl Med*. 2021;13, eabd6434.
42. Dadgar-Kiani E, Bieri G, Melki R, Gitler AD, Lee JH. Mesoscale connections and gene expression empower whole-brain modeling of α-synuclein spread, aggregation, and decay dynamics. *Cell Rep*. 2022;41, 111631.
43. Liebmann T, Renier N, Bettayeb K, Greengard P, Tessier-Lavigne M, Flajolet M. Three-dimensional study of Alzheimer's disease hallmarks using the iDISCO clearing method. *Cell Rep*. 2016;16:1138–1152.
44. Tomris I et al. Distinct spatial arrangements of ACE2 and TMPRSS2 expression in Syrian hamster lung lobes dictates SARS-CoV-2 infection patterns. *PLoS Pathog*. 2022;18, e1010340.
45. Salinas CBG et al. Integrated brain atlas for unbiased mapping of nervous system effects following liraglutide treatment. *Sci Rep*. 2018;8:10310.
46. Secher A et al. The arcuate nucleus mediates GLP-1 receptor agonist liraglutide-dependent weight loss. *J Clin Investig*. 2014;124:4473–4488.
47. Skovbjerg G et al. Uncovering CNS access of lipidated exendin-4 analogues by quantitative whole-brain 3D light sheet imaging. *Neuropharmacology*. 2023;238, 109637.
48. Pan C et al. Deep learning reveals cancer metastasis and therapeutic antibody targeting in the entire body. *Cell*. 2019;179:1661–1676.
49. Mueller JPJ et al. ROCKETS – a novel one-for-all toolbox for light sheet microscopy in drug discovery. *Front Immunol*. 2023;14, 1034032.
50. Pang Z et al. In situ identification of cellular drug targets in mammalian tissue. *Cell*. 2022;185:1793–1805.
51. Nonaka H et al. Revisiting PFA-mediated tissue fixation chemistry: FixEL enables trapping of small molecules in the brain to visualize their distribution changes. *Chem*. 2023;9:523–540.
52. Chen Z, Fan G, Li A, Yuan J, Xu T. rAAV2-Retro enables extensive and high-efficient transduction of lower motor neurons following intramuscular injection. *Mol Ther Methods Clin Dev*. 2020;17:21–33.
53. Duarte F et al. Semi-automated workflows to quantify AAV transduction in various brain areas and predict gene editing outcome for neurological disorders. *Mol Ther Methods Clin Dev*. 2023;29:254–270.
54. Pichardo AH et al. Optical tissue clearing to study the intra-pulmonary biodistribution of intravenously delivered mesenchymal stromal cells and their interactions with host lung cells. *Int J Mol Sci*. 2022;23:14171.
55. Wang Q et al. The Allen mouse brain common coordinate framework: a 3D reference atlas. *Cell*. 2020;181:936–953.
56. Renier N, Adams EL, Kirst C, Dulac C, Osten P, Tessier-Lavigne M. Mapping of brain activity by automated volume analysis of immediate early genes. *Cell*. 2016;165:1789–1802.
57. Alcantara IC, Tapia APM, Aponte Y, Krashes MJ. Acts of appetite: neural circuits governing the appetitive, consummatory, and terminating phases of feeding. *Nat Metab*. 2022;4:836–847.
58. Salinas CBG et al. Integrated brain atlas for unbiased mapping of nervous system effects following liraglutide treatment. *Sci Rep*. 2018;8:10310.
59. Hansen HH et al. Whole-brain activation signatures of weight-lowering drugs. *Mol Metab*. 2021;47, 101171.
60. Rosenstock J et al. Efficacy and safety of a novel dual GIP and GLP-1 receptor agonist tirzepatide in patients with type 2 diabetes (SURPASS-1): a double-blind, randomised, phase 3 trial. *Lancet*. 2021;398:143–155.
61. Falk S et al. GLP-1 and nicotine combination therapy engages hypothalamic and mesolimbic pathways to reverse obesity. *Cell Rep*. 2023;42, 112466.
62. Boland BB et al. Peptide-YY3-36/glucagon-like peptide-1 combination treatment of obese diabetic mice improves insulin sensitivity associated with recovered pancreatic β-cell function and synergistic activation of discrete hypothalamic and brainstem neuronal circuitries. *Mol Metab*. 2022;55, 101392.
63. Petersen J et al. GLP-1-directed NMDA receptor antagonism for obesity treatment. *Nature*. 2024;629:1133–1141.
64. Davoudian PA, Shao L-X, Kwan AC. Shared and distinct brain regions targeted for immediate early gene expression by ketamine and psilocybin. *ACS Chem Neurosci*. 2023;14:468–480.
65. Rijsketic DR et al. UNRAVELing the synergistic effects of psilocybin and environment on brain-wide immediate early gene expression in mice. *Neuropsychopharmacology*. 2023;48:1798–1807.
66. Dedic N et al. TAAR1 agonists improve glycemic control, reduce body weight and modulate neurocircuits governing energy balance and feeding. *Mol Metab*. 2024;80, 101883.
67. Kirschenbaum D et al. Whole-brain microscopy reveals distinct temporal and spatial efficacy of anti-Aβ therapies. *EMBO Mol Med*. 2023;15, e16789.
68. Roostalu U et al. Quantitative whole-brain 3D imaging of tyrosine hydroxylase-labeled neuron architecture in the mouse MPTP model of Parkinson's disease. *DMM Dis Models Mech*. 2019;12, dmm042200.
69. Kirst C et al. Mapping the fine-scale organization and plasticity of the brain vasculature. *Cell*. 2020;180:780–795.
70. Prahst C et al. Mouse retinal cell behaviour in space and time using light sheet fluorescence microscopy. *Elife*. 2020;9, e49779.
71. Jurtz VI et al. Deep learning reveals 3D atherosclerotic plaque distribution and composition. *Sci Rep*. 2020;10:21523.
72. Becher T et al. Three-dimensional imaging provides detailed atherosclerotic plaque morphology and reveals angiogenesis after carotid artery ligation. *Circ Res*. 2020;126:619–632.
73. Schwinn S et al. Cytotoxic effects and tolerability of gemcitabine and axitinib in a xenograft model for c-myc amplified medulloblastoma. *Sci Rep*. 2021;11:14062.
74. Takahashi K et al. Visualization of the cancer cell cycle by tissue-clearing technology using the Fucci reporter system. *Cancer Sci*. 2021;112:3796–3809.
75. Cuccarese MF et al. Heterogeneity of macrophage infiltration and therapeutic response in lung carcinoma revealed by 3D organ imaging. *Nat Commun*. 2017;8:14293.
76. Østergaard MV et al. Automated image analyses of glomerular hypertrophy in a mouse model of diabetic nephropathy. *Kidney360*. 2020;1:469–479.
77. Østergaard MV et al. Therapeutic effects of lisinopril and empagliflozin in a mouse model of hypertension-accelerated diabetic kidney disease. *Am J Physiol-Renal Physiol*. 2021;321:F149–F161.
78. Tahaei E, Coleman R, Saritas T, Ellison DH, Welling PA. Distal convoluted tubule sexual dimorphism revealed by advanced 3D imaging. *Am J Physiol-Renal Physiol*. 2020;319:F754–F764.
79. Kim K et al. Three-dimensional visualization with tissue clearing uncovers dynamic alterations of renal resident mononuclear phagocytes after acute kidney injury. *Front Immunol*. 2022;13, 844919.

80. Gaupp C et al. Reconfiguration and loss of peritubular capillaries in chronic kidney disease. *Sci Rep*. 2023;13:19660.
81. Alvarsson A et al. A 3D atlas of the dynamic and regional variation of pancreatic innervation in diabetes. *Sci Adv*. 2020;6, eaaz9124.
82. Roostalu U et al. 3D quantification of changes in pancreatic islets in mouse models of diabetes type I and II. *Dis Model Mech*. 2020;13, dmm045351.
83. Wu Y-C, Moon H-G, Bindokas VP, Phillips EH, Park GY, Lee S-S-Y. Multiresolution 3D optical mapping of immune cell infiltrates in mouse asthmatic lung. *Am J Respir Cell Mol Biol*. 2023;69:13–21.
84. McKey J, Cameron LA, Lewis D, Batchvarov IS, Capel B. Combined iDISCO and CUBIC tissue clearing and lightsheet microscopy for in toto analysis of the adult mouse ovary. *Biol Reprod*. 2020;102:1080–1089.
85. Pinkert-Leetsch D, Rost JU, Schmiedeknecht MUH, Stadelmann C, Alves F, Missbach-Guentner J. The murine male reproductive organ at a glance: Three-dimensional insights and virtual histology using label-free light sheet microcopy. *Andrology*. 2022;10:1660–1672.
86. Maiuri L et al. Virtual unfolding of light sheet fluorescence microscopy dataset for quantitative analysis of the mouse intestine. *J Biomed Opt*. 2016;21:1.
87. Wang W et al. Three-dimensional quantitative imaging of native microbiota distribution in the gut. *Angewandte Chemie*. 2021;133:3092–3098.
88. Geng J et al. 3D microscopy and deep learning reveal the heterogeneity of crown-like structure microenvironments in intact adipose tissue. *Sci Adv*. 2021;7, eabe2480.
89. Carré D et al. The distribution of neuromuscular junctions depends on muscle pennation, when botulinum neurotoxin receptors and SNAREs expression are uniform in the rat. *Toxicon*. 2022;212:34–41.
90. Glaser AK et al. A hybrid open-top light-sheet microscope for versatile multi-scale imaging of cleared tissues. *Nat Methods*. 2022;19:613–619.
91. Bishop KW et al. An end-to-end workflow for nondestructive 3D pathology. *Nat Protoc*. 2024;19:1122–1148.
92. Nojima S et al. A novel three-dimensional imaging system based on polysaccharide staining for accurate histopathological diagnosis of inflammatory bowel diseases. *Cell Mol Gastroenterol Hepatol*. 2022;14:905–924.
93. Merz SF et al. High-resolution three-dimensional imaging for precise staging in melanoma. *Eur J Cancer*. 2021;159:182–193.
94. Chen Y, Shen Q, White SL, Gokmen-Polar Y, Badve S, Goodman LJ. Three-dimensional imaging and quantitative analysis in CLARITY processed breast cancer tissues. *Sci Rep*. 2019;9:5624.
95. Kaltenecker D et al. Virtual reality-empowered deep-learning analysis of brain cells. *Nat Methods*. 2024;21:1306–1315.
96. Hahn M et al. Mesoscopic 3D imaging of pancreatic cancer and Langerhans islets based on tissue autofluorescence. *Sci Rep*. 2020;10:18246.
97. Roostalu U et al. Quantitative whole-brain 3D imaging of tyrosine hydroxylase-labelled neuron architecture in the mouse MPTP model of Parkinson's disease. *Dis Model Mech*. 2019;12, dmm.042200.
98. Gurdita A et al. InVision: an optimized tissue clearing approach for three-dimensional imaging and analysis of intact rodent eyes. *Iscience*. 2021;24, 102905.
99. Ye Y et al. Visualization of the retina in intact eyes of mice and ferrets using a tissue clearing method. *Transl vis Sci Technol*. 2020;9:1.